J. Fluid Mech. (1975), *vol.* 68, *part* 3, *pp.* 591–608
Printed in Great Britain

Experimental velocity profiles in laminar flow around spheres at intermediate Reynolds numbers

By L. E. SEELEY,† R. L. HUMMEL AND J. W. SMITH

Department of Chemical Engineering and Applied Chemistry, University of Toronto

(Received 16 July 1973 and in revised form 27 May 1974)

Normal and tangential velocities in the boundary layer and out into the free stream have been obtained using a non-disturbing flow visualization technique for uniform laminar flow around a sphere. The non-similar data are available in tables at 2·5° intervals from 20° from the front to about 15° past the separation point at Reynolds numbers of 290, 750, 1300 and 3000. Stream functions calculated by LeClair using a numerical solution of the Navier–Stokes equation at $Re \simeq 300$ are not in good agreement with measured values from 30° to 60°, but are in much better agreement around the separation point. Too few grid points near the sphere where the tangential velocities rise to a maximum above free-stream values may account for the difference.

1. Introduction

The dynamics of fluid flow around spheres is a classical problem, but analytical solutions of the Navier–Stokes and continuity equations are feasible only when viscous forces predominate, i.e. $Re < 1$. 'Exact' and approximate numerical solutions (Hamielec, Hoffman & Ross 1967; Jenson 1959; LeClair 1970; LeClair & Hamielec 1970; LeClair, Hamielec & Pruppacher 1970; Pruppacher, LeClair & Hamielec 1970; Rimon & Cheng 1969) are available up to $Re = 1000$ but these have not been checked against experimental velocity data at any flow rate. Son & Hanratty (1969) and LeClair (1970) have pointed out that stability of the non-linear second-order difference equation in the computational methods does not necessarily mean that the numerical solution has converged to the exact solution of the nonlinear second-order partial differential equation. In reducing the latter equation to a nonlinear algebraic equation, in imposing certain boundary conditions, in setting the relaxation mesh to specific systematic values and in imposing a specific relaxation method, some approximation will result.

Boundary-layer theory has been applied with some success for $Re > 3000$, when inertial forces are expected to predominate, and Knapp & Roache (1968), Frossling (1958), Lee & Barrow (1968), Linton & Sutherland (1960), Locheil & Calderbank (1964) and Tang, Duncan & Schweyer (1953) have applied the theory in the intermediate Reynolds number range 1–3000. Hamielec *et al.* (1967) have

† Present address: Falconbridge Nickel Mines, Ltd, Sudbury, Ontario, Canada.

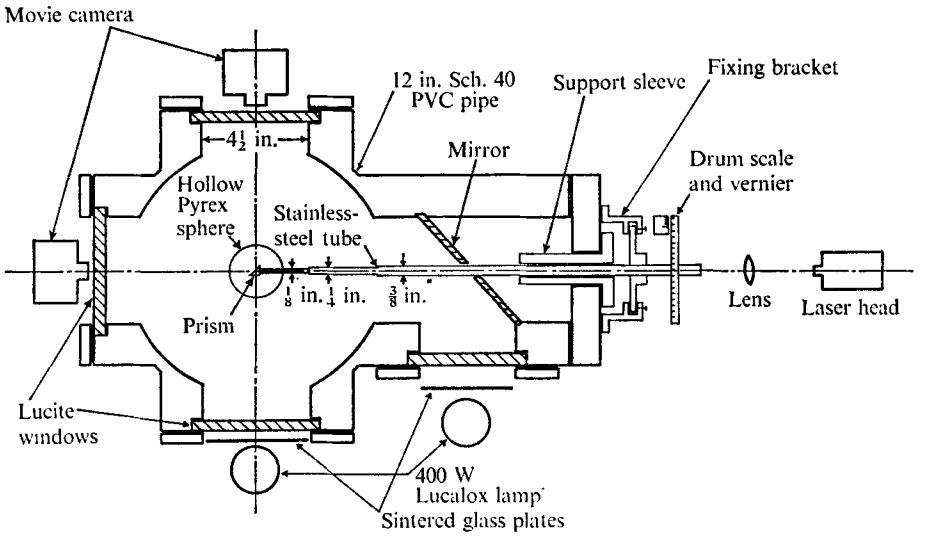

FIGURE 1. Top view of test section.

stated that boundary-layer theory reasonably describes flow around a sphere for *Re* as low as 100, but no experimental velocity data are available to confirm this claim.

Fundamental microscopic experimental velocity data for flow around spheres have not been obtained until recently because of experimental difficulties involved. A non-disturbing technique which depends on the formation of a visible time line in the test fluid by irradiation of a photochromic indicator substance dissolved therein at any desired angle to the direction of flow has been developed and is described by Popovich & Hummel (1967), Iribarne *et al.* (1969) and Smith & Hummel (1973). Steady one-dimensional flow velocities may be obtained by analysis of high-speed photographs, and two-dimensional flow fields may be obtained by use of a mass balance. Microscopic qualitative observations can also be made at the front stagnation point, in the laminar boundary layer and at the separation point.

2. Experiment

The experimental equipment is described in detail by Seeley (1972) and consisted of a metered flow circuit whereby the test fluid, Shell-sol 715 kerosene in which the photochromic indicator 1,3,3-trimethylindolino-6′-nitrobenzopyrylospiran (TMINBPS) and an antistatic agent Shell ASA-3 were dissolved, could be circulated past the test sphere. A top view of the test section is shown in figure 1. Blue dye traces, normal to the sphere and at different angles from the front stagnation point, were initiated nearly instantaneously (in $< 10^{-6}$ s) in the clear Newtonian liquid by passing a focused beam of ultra-violet light (3472 Å) from a giant pulse ruby laser with a frequency doubler through the holder of the hollow Pyrex sphere and through a 90° prism located at the centre of the sphere. The line

Composition	99·9 % paraffins
Flash point	51 °C
Conductivity	410 pΩ/m
Density at 23 °C	0·753 g/cm³
Viscosity at 23 °C	1·35 cP
Refractive index at 23 °C	1·4232

TABLE 1. Properties of test fluid

trace formed by the phototropic reaction of the indicator induced by UV light was photographed simultaneously by two 16 mm movie cameras as it deformed with the flow. Fluid velocities were obtained from the resulting displacement of the dye trace with time and from the continuity equation.

Throughout, $\frac{3}{8}$ in. diameter honeycombs, perforated lucite plates and screens were used to reduce turbulent fluctuations to less than 0·5% in the 12 in. diameter, 24 in. long circular cylindrical test section.

The angle of the trace from the front stagnation point was measured with a drum scale and vernier accurate to 0·1°.

The spheres were blown from round-bottommed Pyrex flasks. A 90° borosilicate crown optical glass prism with an antireflexion coating (magnesium fluoride) was glued to the end of a $\frac{1}{8}$ in. diameter stainless-steel tube and located in the centre of each sphere. The stainless-steel tube was glued to the glass sphere. The sphere was rounded up at the sphere holder with epoxy and smoothed and polished in a lathe. Stainless-steel tubes $\frac{1}{4}$ and $\frac{3}{8}$ in. in diameter were then glued to the $\frac{1}{8}$ in. tube as shown in figure 1. Two spheres of diameter 6·008 cm and 3·495 cm were used in this study.

The laser head was mounted on a lathe-bed which permitted movement in all three directions. The frequency-doubled laser beam was focused using a thin plano-convex lens.

The traces formed were photographed by Bolex H16 Reflex and Bolex Paillard cameras operating simultaneously and mutually perpendicular to each other. Illumination was by 400 W lucalox lamps using d.c. rectifiers.

The test solution containing 0·01 % by weight TMINBPS and 6 p.p.m. ASA-3 additive was characterized and some of the results are given in table 1. The solution obeyed Beer's law for a low concentration of indicator (up to 0·04 %), showing that no micelles or agglomerates were formed by the indicator. Tests with a Fann viscometer showed that the solution was Newtonian.

The laser was fired 4–7 times for each setting in laminar flow and at least 7000 instantaneous velocities were obtained from the traces for each *Re*. The traces were photographed at the front stagnation point and at 15° intervals from the front stagnation point to the rear stagnation point, about which intervals were reduced to 10°. For many of the close-up shots the traces could be followed for 15°–20° as they flowed around the sphere.

Reynolds numbers of 750, 1300 and 3000 were studied with the 6·008 cm sphere and Reynolds numbers of 1300 and 290 with the 3·495 cm sphere.

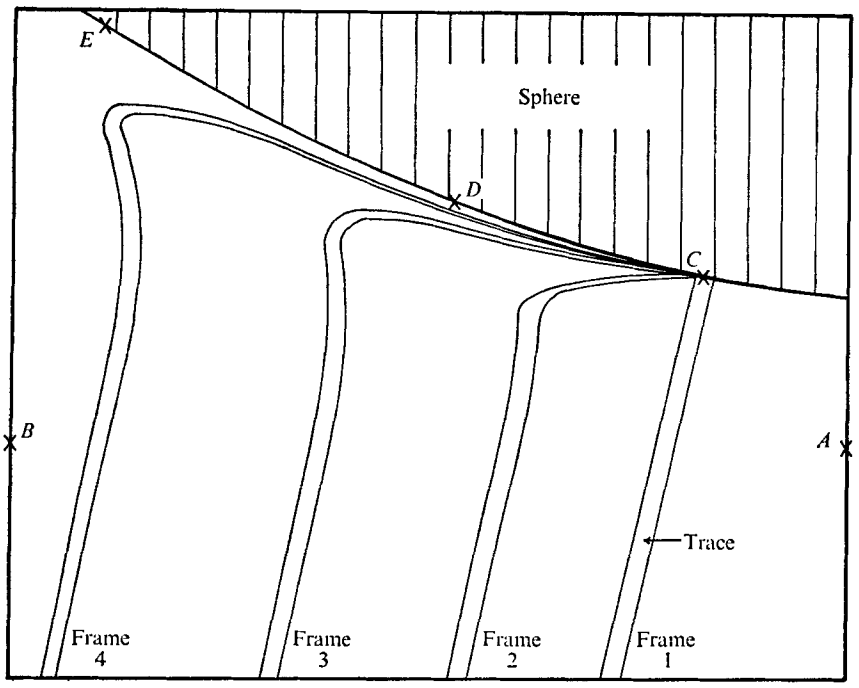

FIGURE 2. Schematic diagram of trace flowing around sphere.

Data processing and storage

(X, Y) co-ordinates for the dye traces were read from the films by projecting frame by frame onto a screen with a 1 cm grid (70 × 50 cm) and transferred to computer cards.

The following quantities were recorded.

(1) Magnification from the frame size (points A and B in figure 2).

(2) For the first frame in a sequence, the centre (X'', Y'') of the dye trace at the edge of the sphere at point C in figure 2.

(3) The co-ordinates of two points D and E on the sphere surface. C, D and E were then used to determine the sphere centre.

(4) The (X, Y) co-ordinates of the centre-line of the trace on the first frame, the points being chosen to ensure adequate representation of the curve by linear interpolation.

(5) Frames 2, 3, 4, etc., were read as in step 4. The frame number was noted to determine the time scale.

(6) Steps 1–5 were repeated for each shot. End views of the traces were logged in the same way.

The data were transformed into spherical co-ordinates as shown in figure 3. Raw data are represented by the projected system (X'', Y''). To transform these data to the co-ordinate system (X', Y') based on the sphere centre, the location of the centre in the (X'', Y'') system was determined from C, D and E knowing AB and the radius R. The equations of a circle with centre O were solved simultaneously for C and E by the generalized Newton–Raphson method. The

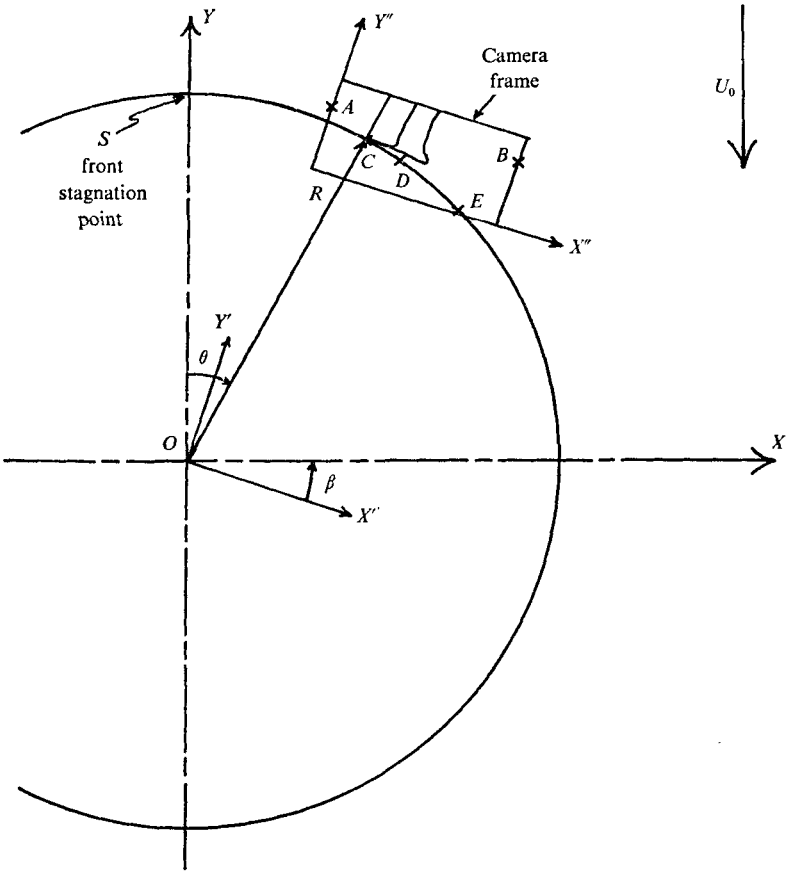

FIGURE 3. Schematic diagram of transformation of co-ordinates.

middle point D was used to determine the correct solution and to check the accuracy of the solution by calculating the radius OD and comparing it with R. The agreement was excellent, the standard error being less than 0·001 cm for $R = 3{\cdot}0$ cm. The co-ordinates of the centre were labelled (X_T, Y_N) with respect to the (X'', Y'') system.

The new co-ordinate system (X', Y') was then rotated through an angle β so that the Y axis passed through the front stagnation point S. The angle β was determined by the generalized Newton–Raphson method from the equation of the circle through C with centre O and the equation

$$\tan(90-\theta) = Y_0/X_0, \tag{1}$$

where (X_0, Y_0) are the co-ordinates of C with respect to co-ordinate axes X and Y. θ is the angle from the front stagnation point. The transformation was completed for spherical co-ordinates using the equations

$$X = (X''-X_T)\cos\beta-(Y''-Y_N)\sin\beta, \tag{2}$$

$$Y = (Y''-Y_N)\cos\beta+(X''-X_T)\sin\beta, \tag{3}$$

$$r = X^2+Y^2, \tag{4}$$

$$\theta = \tfrac{1}{2}\pi-\arctan(Y/X). \tag{5}$$

Tangential and radial velocities were then calculated by the following iterative procedure.

(1) Streamlines very close to the spheres were assumed to be tangential to the sphere surface. Typically, a radial spacing $\Delta(r-R)/R$ or Δy of 0·003 was chosen near the sphere, increasing to 0·024 at $y > 0{\cdot}099$.

(2) Trace readings in the first radial position were linearly interpolated to obtain θ co-ordinates.

(3) Tangential velocities were calculated in the first radial position assuming no radial motion. Instantaneous velocities deviating by more than 4σ from the mean were discarded.

(4) The 'normal velocity' was determined from a mass balance on radial elements of size $\Delta\theta = 1°$ by Δy and fitted with a seventh-order regression equation.

(5) Tangential velocities were recalculated from the original trace data using the regression-fit expression for the normal velocity

(6) Streamlines were determined interatively at the area-average radial position and average tangential velocities calculated.

(7) Steps 3–6 were repeated until constant velocities were obtained, usually after 2–5 interations.

(8) The final velocity data, regression polynomials, the standard deviation about the regression polynomials and the radial position were obtained as print-outs, punched cards and Calcomp plots.

(9) Steps 1–8 were repeated at the next radial position using normal velocity data from the preceding radial position.

3. Error

Errors in the application of this technique in laminar flow can be assigned to the following.

(*a*) Convective movement of the trace due to local heating.

(*b*) Random turbulent motions in the free stream.

(*c*) The reading error, i.e. the error arising when the centre-line of a finite trace is determined.

(*d*) Random experimental errors, such as arise from determining the magnification, reading the rotameters, measuring temperature and setting the trace angle and camera speed.

(*e*) Computational and processing errors, affected by the goodness of fit of the polynomial regression and the procedures for linearization and interpolation.

(*f*) The effect of the sphere support.

Dye traces formed in the stationary test fluid showed no measurable motion due to natural convection. As discussed in the subsequent sections, residual turbulence in the free stream was found to be no more than 0·1–0·5% and the sphere holder had a negligible effect in the range of Re studied.

Dunn & Smith (1972) analysed the effect of random reading and experimental errors for laminar and turbulent flow in smooth and rough pipes using this technique. They found that a laminar profile could be measured with a standard

precision of $\pm 1\%$ at the centre-line and of $\pm 5\%$ near the wall of a $\frac{1}{2}$ in. glass tube. A similar reliability can be expected in the determination of the trace position in this study.

In two-dimensional flows, additional computations and a mass balance are required to find the tangential and radial velocities. By keeping the linearized and interpolated distances small, the standard error in this procedure was kept to less than $\pm 4\%$. The standard error of the mean caused by the goodness of fit in regression analysis was estimated to be about ± 3–4% near the sphere and ± 1–2% in the free stream. The standard error in flow rates measured by the probe is ± 2–3%, and the estimated standard error in the angular distances is about $\pm 0{\cdot}5°$.

In total, the standard error in the mean velocities, which are regression-fit averages of the instantaneous velocities, is about $\pm 13\%$ near the sphere and $\pm 5\%$ in the main stream.

Confidence in the results is increased by the fact that the tangential velocity profiles relaxed to the correct and independently measured free-stream values (see figures 9 and 11) in all experiments where the traces were long enough.

4. Results and discussion

Velocity profiles in open test section

Uniformity of flow in the test section was checked using an optical probe without a sphere at several velocities and distances from the centre-line. Figure 4 (plate 1) shows a typical sequence of frames. Flat velocity profiles were obtained at the flow rates used in this study. The standard error in the horizontal displacement of the dye trace is $0{\cdot}1$–$0{\cdot}5\%$, and is made up of the reading error and turbulence. Hence the turbulence intensity was no more than $0{\cdot}1$–$0{\cdot}5\%$ and probably much less.

Qualitative flow observations

Front stagnation point to the wake. Several thousand feet of 16 mm film were observed and some representative frames are given in figures 5 and 6 (plates 2 and 3). The time scale, the angle of the trace at initiation, the diameter of the sphere, the sphere Reynolds number and the vertical height L_e of the picture in the physical system are given in the captions to all photographs; the flow direction of the main stream is downwards.

The flow at the front was axisymmetric at a Reynolds number of 760 as shown in figure 5. For $Re < 290$ a rotation in the wake about the axis of symmetry was transmitted to the front of the sphere, and quantitative measurements could not be made. The fluid in the region of the front stagnation point was of low velocity and became part of the boundary layer. In laminar flow, a laminar boundary layer developed which rapidly thickened as the separation point was reached (cf. figures 5 and 6). No turbulent disturbance was ever seen in the boundary layer or the free stream.

Figure 5 (*b*) shows a characteristic acceleration and development of a maximum tangential velocity above the free-stream value within the boundary layer. Such

Re	Separation angle, θ_s (deg)
290	120·9
760	111·5
1235	103·9
1300	102·5
2940	96·0

TABLE 2. Separation angles

a maximum has been postulated by Libby & Liu (1967), and is to be expected since the fluid will tend to accelerate to the potential flow velocity rather than the undisturbed free-stream velocity.

Flow in the wake. The flow pattern in the wakes at $Re = 155$, 290 and 760 was seen to be affected to some extent by the sphere holder, which caused non-axisymmetric rotation and circulations at sphere-to-support diameter ratios D/d of 18·8 and 10·9.

Taneda (1956) reported that a support normal to the flow for $D/d = 30$ had a negligible effect on the wake for sphere Reynolds numbers from 5 to 300. Raithby & Eckert (1968) showed that a cross-flow support with $D/d = 9{\cdot}45$ had a negligible effect on flow over the front of the sphere but caused asymmetry in the wake in the range of Re studied (20 000–250 000). Kalra & Uhlherr (1971) reported that the separation angle and wake dimensions were unaffected by the sphere support for D/d from 8·8 to 36 and for Re from 30 to 750. Wake dimensions were not measured in this study, but the separation angles θ_s in table 2 were reasonably correlated by Kalra & Uhlherr's (1971) equation

$$\theta_s - 83 = 262\, Re^{-0{\cdot}372}. \tag{6}$$

The best correlation was found with the equation of Linton & Sutherland (1960) based on their own data:

$$\theta_s - 83 = 660\, Re^{-0{\cdot}5}. \tag{7}$$

At $Re = 290$ the circulation could not be detected at the separation point but was pronounced at the rear stagnation point. Oscillations with the magnitude of the sphere radius were associated with the movement downstream of large vortices which formed periodically about $1{\cdot}5R$ downstream. Fluid from the main stream was entrained in the wake after each vortex was shed. Near the sphere, the wake flow was laminar and of low velocity relative to the main stream.

At $Re = 760$, vortex shedding was faster and the scale of the vortices much smaller. Pulsations from the shedding process were not observed at the sphere surface. The laminar boundary layer separated smoothly and was undisturbed until reaching the region of vortex shedding, where it was entrained in the vortices. Flow within the wake was laminar.

At $Re = 1300$, large- and small-scale jets and eddies associated with a three-dimensional rotation appeared in the wake. These fluctuations resulted in a continual change in direction and magnitude of velocities near the surface of the sphere. Occasionally low amplitude waves formed in the free shear layer about

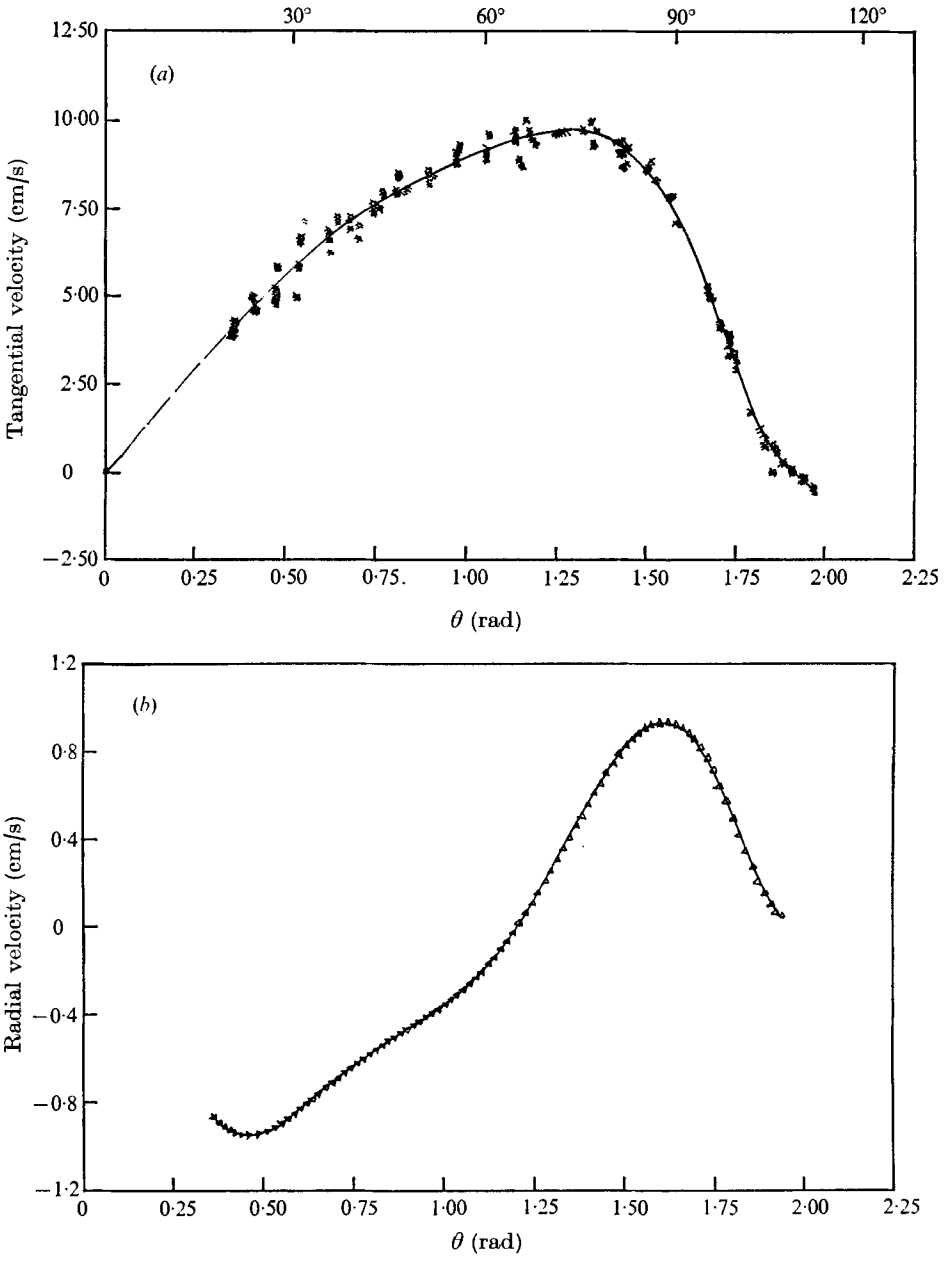

FIGURE 7. (*a*) Tangential and (*b*) radial velocities against θ; $Re = 2940$, $y = 0{\cdot}063$, $V_0 = 8{\cdot}87$ cm/s, $\theta_s = 1{\cdot}68$ rad.

half a sphere diameter downstream which at times amplified to form an eddy or eddies. At other times, the free shear layer was accelerated into the reattachment zone with the formation of eddies. Infrequently, these eddies did not move downstream but were entrained in the wake. The formation of an eddy usually resulted in the rapid appearance of other eddies, both larger and smaller.

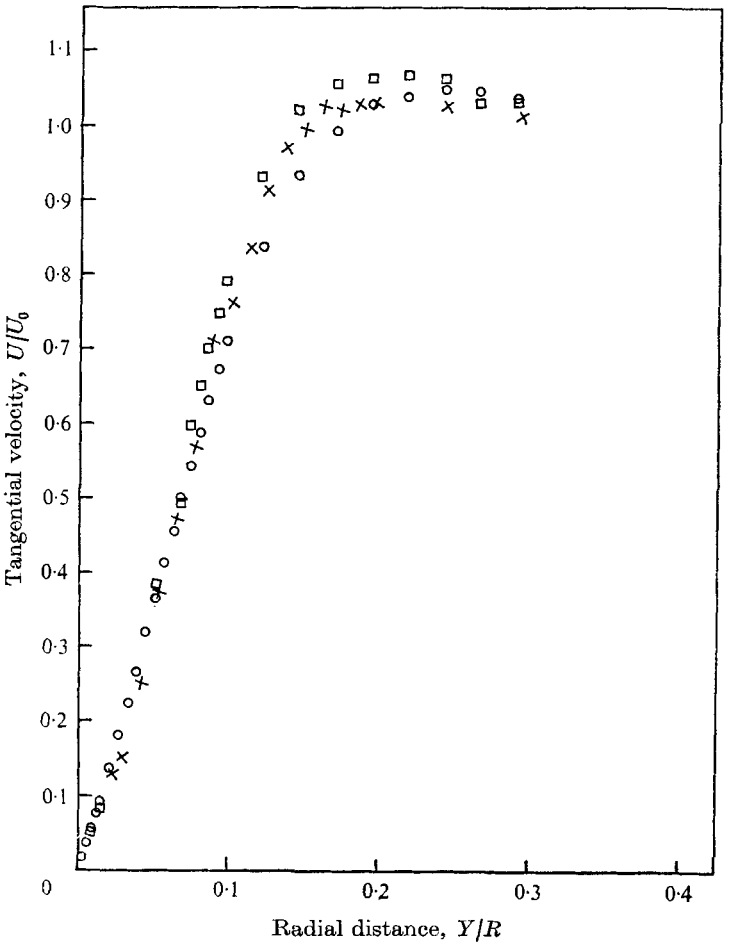

FIGURE 8. Effect of sphere support on flow field. □, Re = 1300, normal flow plane; ×, Re = 950, flow field 180° from support; ○, Re = 760, normal flow plane.

At Re = 2940, the fluctuations within the wake became more intense and of smaller scale. Waves in the free shear layer formed closer to the separation point, were of higher frequency and magnitude and formed vortices which amplified rapidly and moved downstream.

Experimental velocity profiles

A sample selected from some 70 graphs of tangential and radial velocity data with the polynomial regression curves has been reproduced from Calcomp plots in figures 7 (*a*) and (*b*) for Re = 2940 at a dimensionless radial distance of 0·063. These data have been reduced to tables of tangential and radial velocities at 2·5° intervals starting at 20° from the front stagnation point and continuing to about 15° past the separation point. Depending on the dye trace, from 25 to 50 radial positions beginning at a minimum dimensionless radial distance of 0·003 from the surface are given for each profile.

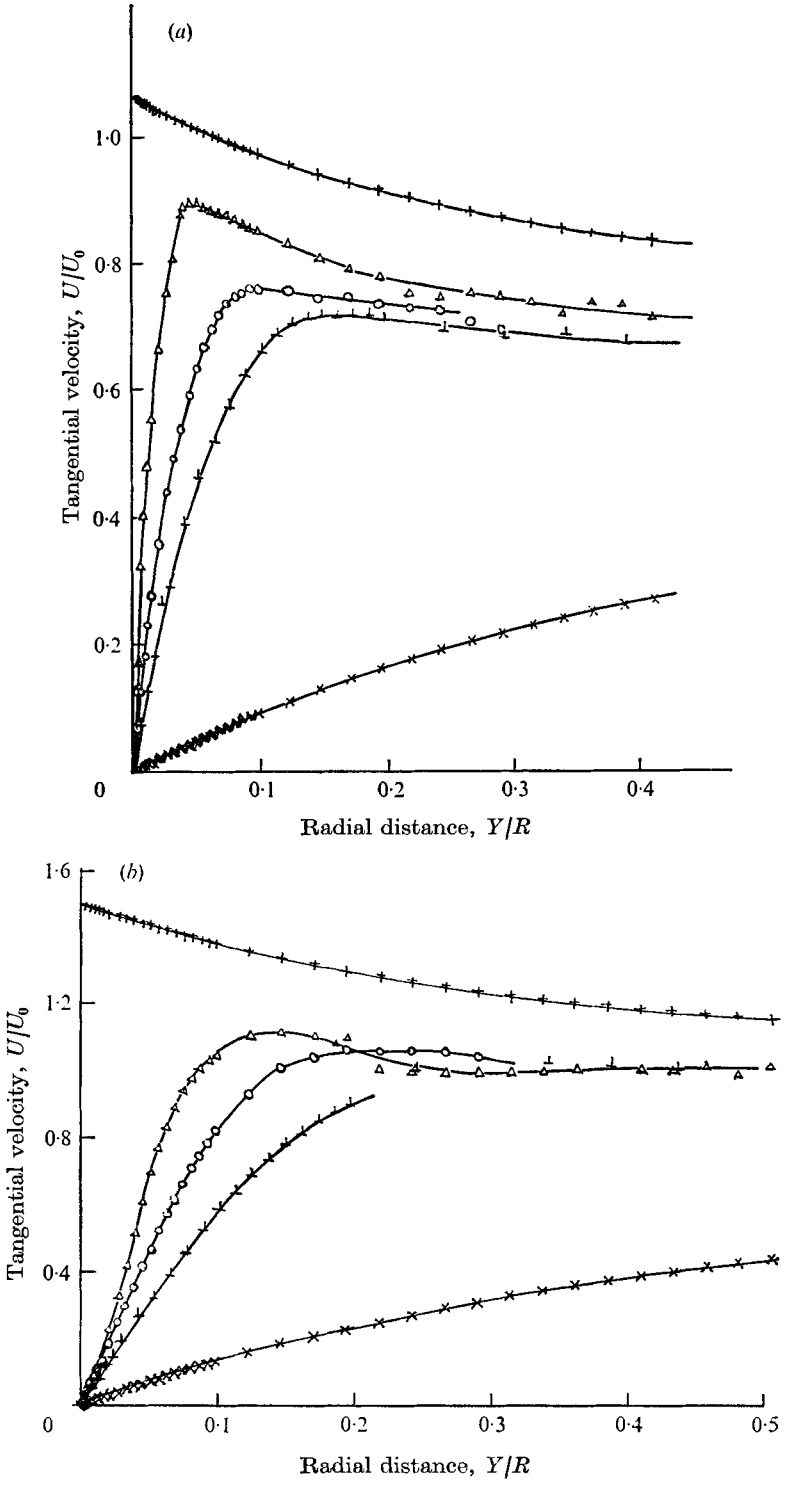

FIGURES 9(*a*, *b*). For legend see next page.

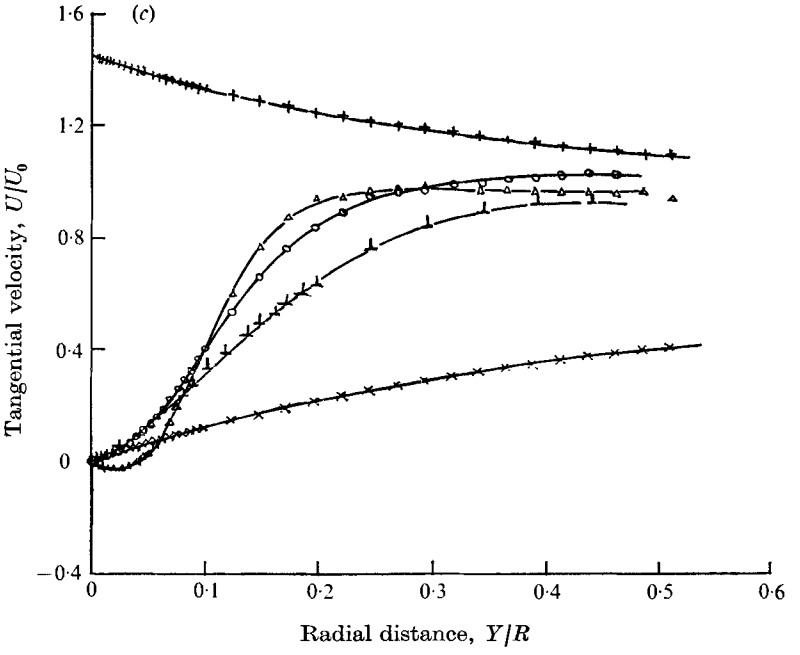

FIGURE 9. Tangential velocities against Y/R. +, potential; ×, Stokes; △, Re = 2940; ○, Re = 760; ⊥, Re = 290. (*a*) θ = 45°. (*b*) θ = 90°. (*c*) θ = 105°.

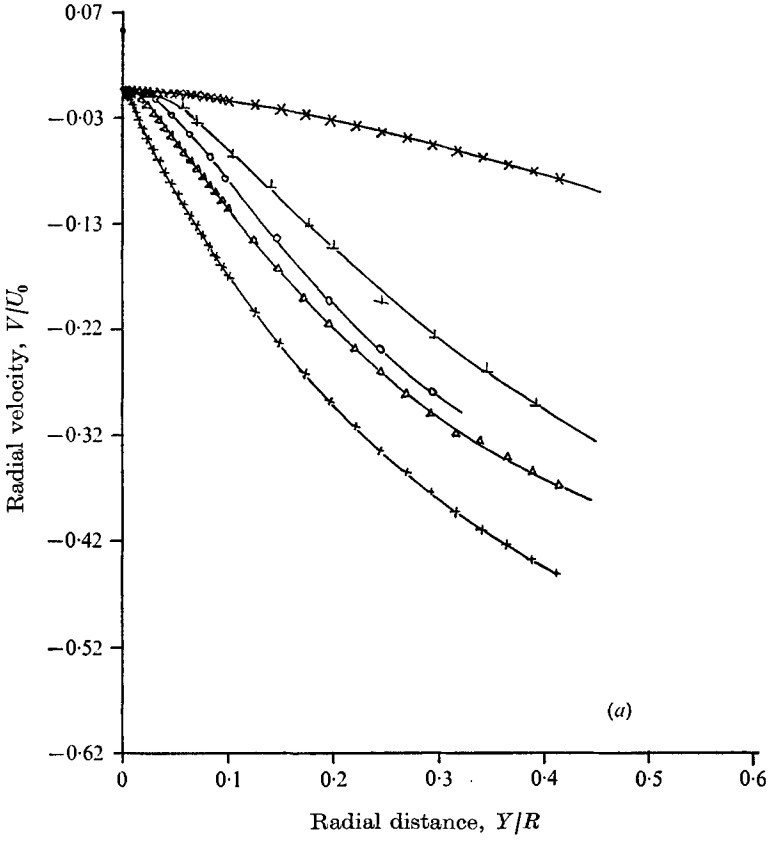

FIGURE 10(*a*). For legend see facing page.

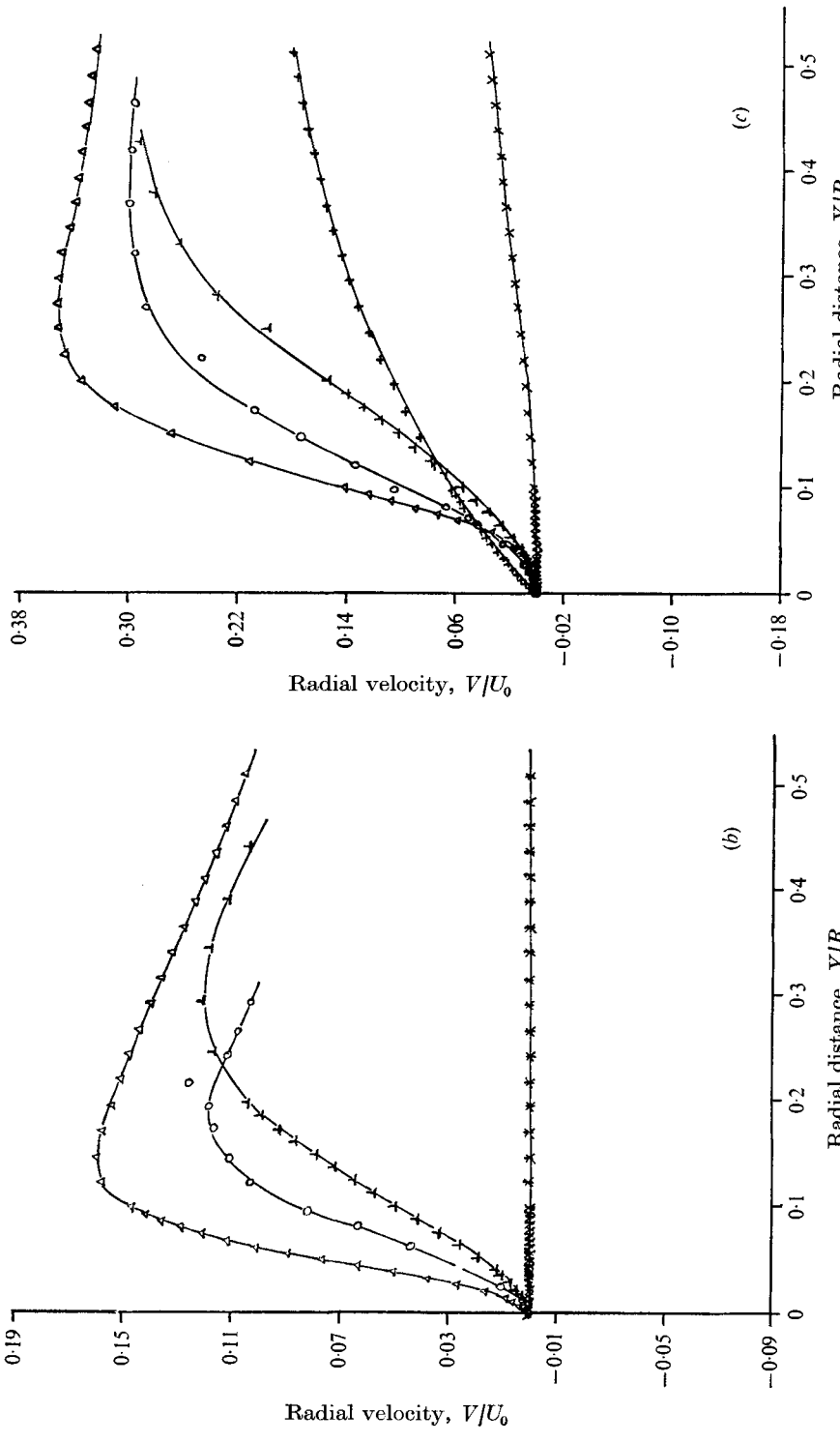

FIGURE 10. Radial velocities against Y/R. Symbols as in figure 9. (*a*) $\theta = 45°$. (*b*) $\theta = 90°$. (*c*) $\theta = 105°$.

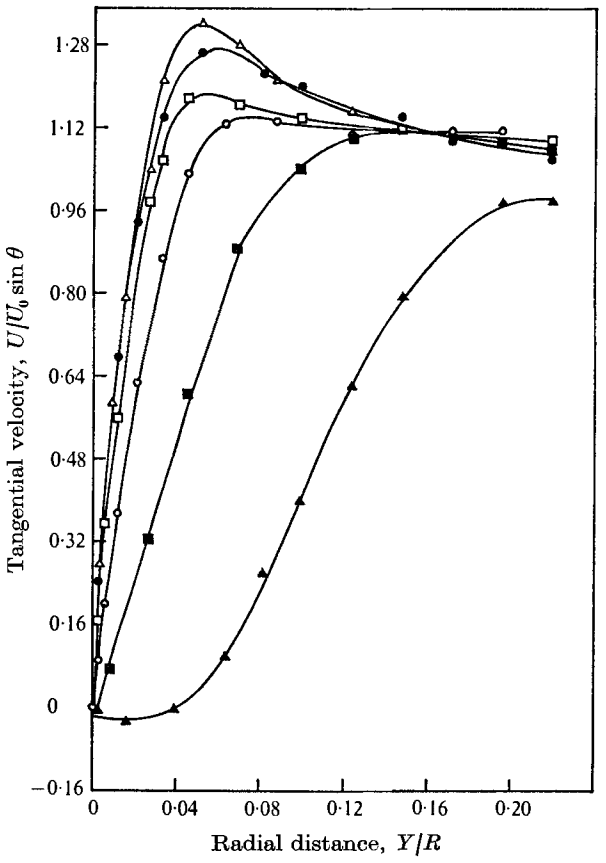

FIGURE 11. Tangential velocities normalized by $\sin\theta$ *vs.* Y/R. Re = 2940. θ: △, 30°; ●, 45°; □, 60°; ○, 76°; ■, 90°; ▲, 105°.

Although the sphere holder did not appear to have any effect on flow in front of the wake for $Re > 290$, the possibility of quantitative effects was checked by making measurements at 90° from the front stagnation point in a vertical plane including the sphere holder. Flow was ordinarily studied in a vertical plane normal to the sphere holder. Figure 8 shows that the tangential velocity data obtained for similar Reynolds numbers are nearly identical.

Representative plots of tangential velocities from these experimental data at 45°, 90° and 105° are presented in figures 9 (*a*)–(*c*) and the corresponding radial velocities in figures 10 (*a*)–(*c*). Stokes and potential flow solutions are shown as a basis for comparison. Figure 11 gives the non-similar tangential profiles normalized as $U/U_0 \sin\theta$ against radial distance for Re = 2940.

These plots show the development of a 'spike' in the tangential velocities greater than the free-stream values and the subsequent relaxation of the velocities down to the free-stream value. Clearly, in the intermediate Re range, the application of the potential flow solution as the outer boundary condition for the boundary layer is inappropriate at small δ/R, although most models for

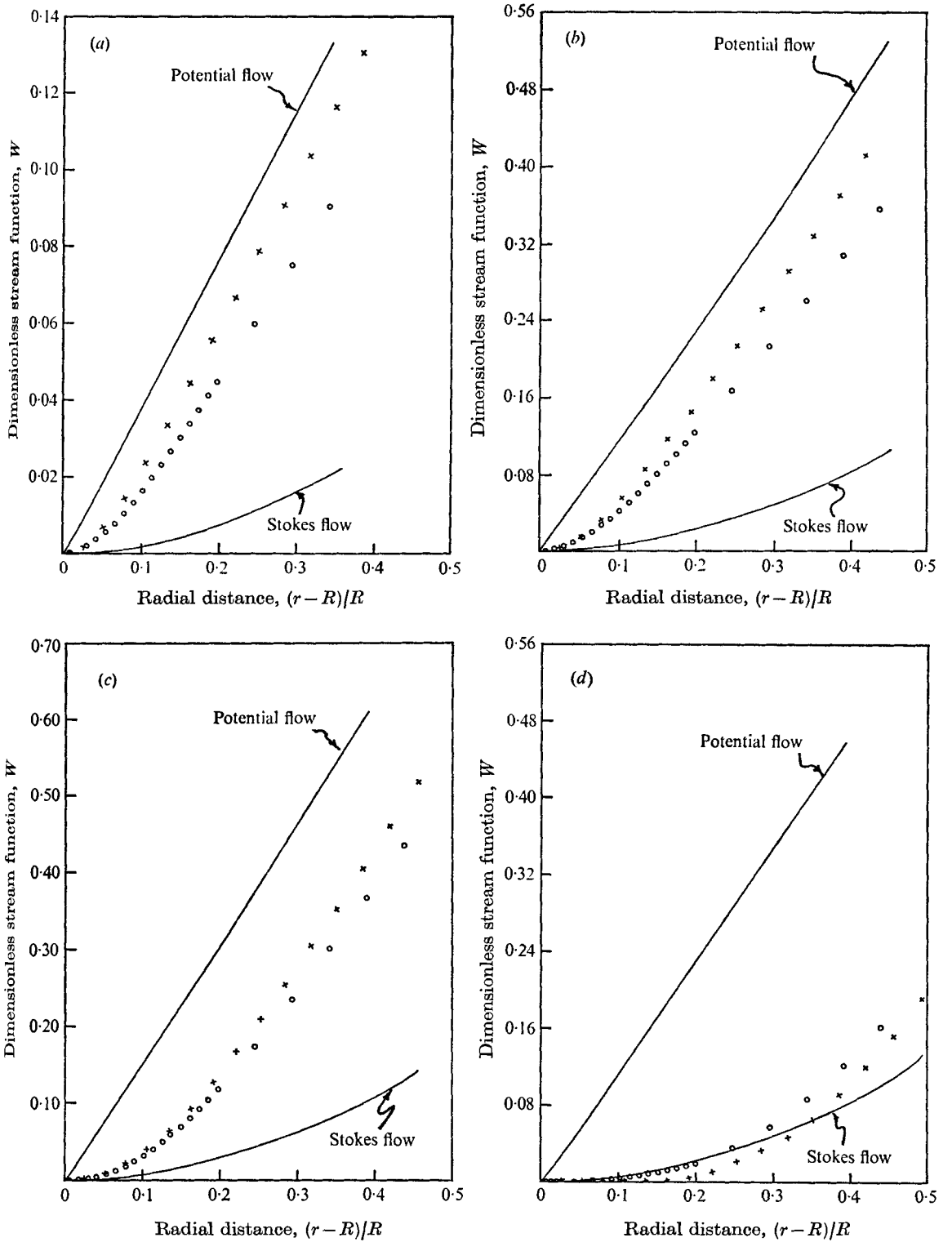

FIGURE 12. Dimensionless stream function W against radial distance. (*a*) $\theta = 30°$. (*b*) $\theta = 60°$. (*c*) $\theta = 90°$. (*d*) $\theta = 120°$. ○, this work, $Re = 290$; ×, LeClair, $Re = 300$.

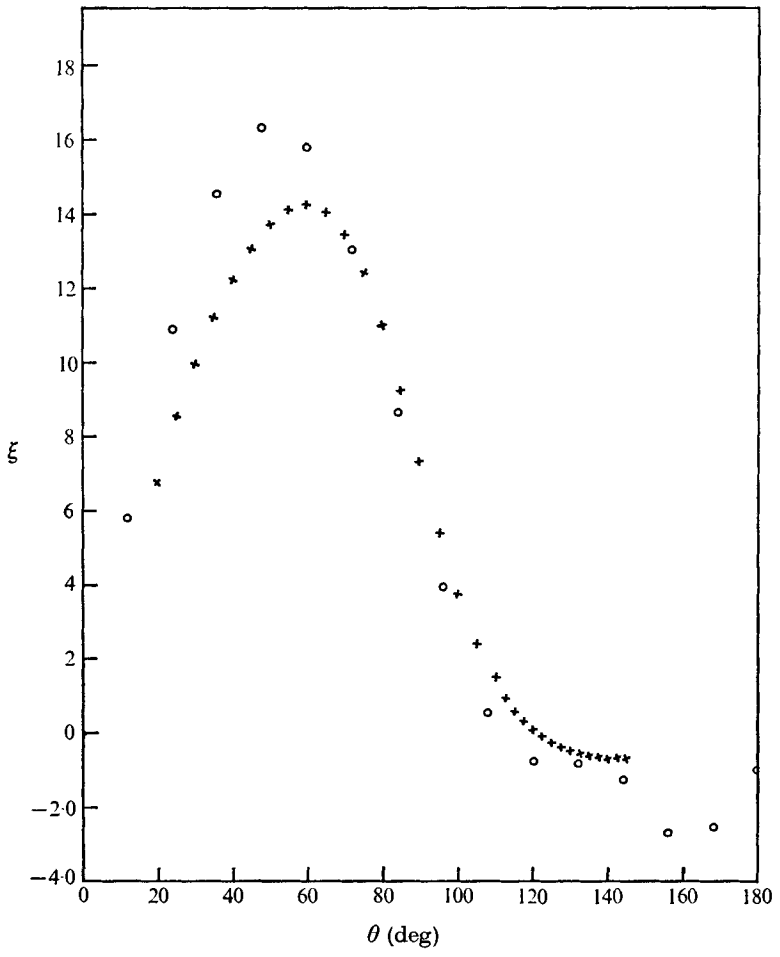

FIGURE 13. Surface vorticity ξ. ×, measured, Re = 290; ○, calculated by LeClair, Re = 300.

mass and heat transfer are based on this condition. The assumption that the boundary-layer thickness is much less than the sphere radius is inappropriate since δ/R varies from 0·05 to more than 0·4, depending on θ and R.

The radial velocity profiles at 45° (figure 10 (*a*)) show a transition from Stokes type to potential flow type profiles with increasing Reynolds number, but at 90°, the measured V/U_0 values do not lie between the analytical curves because the effective shape of the sphere is changed by the boundary layer. Near the wall, the measured radial velocities correctly approach zero asymptotically.

Numerical solutions of the Navier–Stokes equations are available up to $Re \simeq 1000$, but have not been calibrated against experimental velocity data. As pointed out by Masliyah & Epstein (1970) and Torobin & Gauvin (1959) comparisons of overall drag coefficients, separation points and wake dimensions are relatively insensitive to changes in the flow field.

Dimensionless stream functions W at angles of 30°, 60°, 90° and 120° are

compared in figures 12 (*a*)–(*d*), using LeClair's (1972, private communication) values at $Re = 300$ and measured values at $Re = 290$. In view of the insensitivity of the stream function to changes in the velocity field, agreement is surprisingly only fair at $\theta = 30°$ and 60°, and the difference of about 25 % at 30° is too large to be due to random experimental error. The relatively poor agreement is possibly due to the grid scheme used in LeClair's and other work. The scheme was based on the equation $\Delta r = e^Z \Delta Z$. LeClair (1970) used $\Delta Z = 0{\cdot}025$ and $\Delta\theta = 3°$ for calculations at $Re = 300$ and Rimon & Cheng (1969) used $\Delta Z = 0{\cdot}05$ and $\Delta\theta = 6°$. At $\theta = 30°$ and $Re = 300$ experimental data show that LeClair would have only six grid points within the viscous boundary layer and Rimon & Cheng would have only three. At $Re = 1000$, Rimon & Cheng would have only one point in the viscous layer. More grid points are probably required to map the maximum in the tangential velocity with the subsequent decrease to the free-stream value found experimentally but not revealed by differentiation of the stream function.

The plot of surface vorticity against θ at $Re = 300$ in figure 13 also shows a significant difference between experimental and calculated values in the range of θ from 30° to 60°.

The data provided by this study may be used quite conveniently to calculate pressure profiles and properties arising in boundary-layer theory. Some of these calculations have been made by Seeley (1972), but are not presented here. In general, agreement between boundary-layer values and experimental ones was either poor or fortuitous in the range of Re studied.

5. Conclusion

Tangential and normal velocity data have been obtained for uniform laminar flow around a sphere at Reynolds numbers of 290–2940 from an angle of about 20° from the front stagnation point to approximately 15° downstream of the separation point. This is the first time such data have been presented in the accessible literature for any range of sphere Reynolds numbers, and this range in particular, or for other bluff bodies such as cylinders. The need for and value of this type of data, especially for calculating mass and heat transfer rates and for calibration of numerical and boundary-layer solutions, are well known.

The authors are grateful to the National Research Council of Canada and the Canadian International Development Agency for financial support, and to A. Iribarne, V. Arunachalam, F. Frantisak, O. Trass and others for assistance of various kinds along the way

REFERENCES

Dunn, S. G. & Smith, J. W. 1972 *Can. J. Chem. Engng*, **50**, 561.

Frossling, N. 1958 *N.A.C.A. Tech. Memo.* no. 1432.

Hamielic, A. E., Hoffman, T. W. & Ross, L. L. 1967 *A.I.Ch.E. J.* **13**, 212.

Iribarne, A. deP., Hummel, R. L., Frantisak, F. & Smith, J. W. 1969 *Chem. Engng Prog.* **65**, 60.

JENSON, V. G. 1959 *Proc. Roy. Soc.* A **249**, 346.

KALRA, T. R. & UHLHERR, P. H. T. 1971 *4th Aust. Conf. on Hydraul. & Fluid Mech., Monash University.*

KNAPP, C. F. & ROACHE, P. J. 1968 *A.I.A.A. J.* **6**, 29.

LECLAIR, B. P. 1970 Ph.D. thesis, Chem. Engng, McMaster University, Hamilton, Ontario.

LECLAIR, B. P. & HAMIELEC, A. E. 1970 *Fluid Dyn. Symp., McMaster University, Hamilton, Ontario.*

LECLAIR, B. P., HAMIELEC, A. E. & PRUPPACHER, H. R. 1970 *J. Atmos. Sci.* **27**, 308.

LEE, K. & BARROW, H. 1968 *Int. J. Heat Mass Transfer*, **11**, 1013.

LIBBY, P. A. & LIU, T. M. 1967 *A.I.A.A. J.* **5**, 1040.

LINTON, M. & SUTHERLAND, K. L. 1960 *Chem. Engng Sci.* **12**, 214.

LOCHEIL, A. C. & CALDERBANK, P. H. 1964 *Chem. Engng Sci.* **19**, 471.

MASLIYAH, J. H. & EPSTEIN, N. 1970 *J. Fluid Mech.* **44**, 493.

POPOVICH, A. T. & HUMMEL, R. L. 1967 *Chem. Engng Sci.* **22**, 21.

PRUPPACHER, H. R., LECLAIR, B. P. & HAMIELEC, A. E. 1970 *J. Fluid Mech.* **44**, 781.

RAITHBY, G. D. & ECKERT, E. R. G. 1968 *Warme & Stoffubertragung*, **1**, 87.

RIMON, Y. & CHENG, S. I. 1969 *Phys. Fluids*, **12**, 949.

SEELEY, L. E. 1972 Ph.D. thesis, Chem. Engng Dept., University of Toronto.

SMITH, J. W. & HUMMEL, R. L. 1973 *J. S.M.P.T.E.* **82**, 278.

SON, J. S. & HANRATTY, T. J. 1969 *J. Fluid Mech.* **35**, 369.

TANEDA, S. 1956 *J. Phys. Soc. Japan*, **11**, 1104.

TANG, Y. S., DUNCAN, J. M. & SCHWEYER, H. E. 1953 *N.A.C.A. Tech. Note*, no. 2867.

TOROBIN, L. B. & GAUVIN, W. H. 1959 *Can. J. Chem. Engng*, **37**, 129.

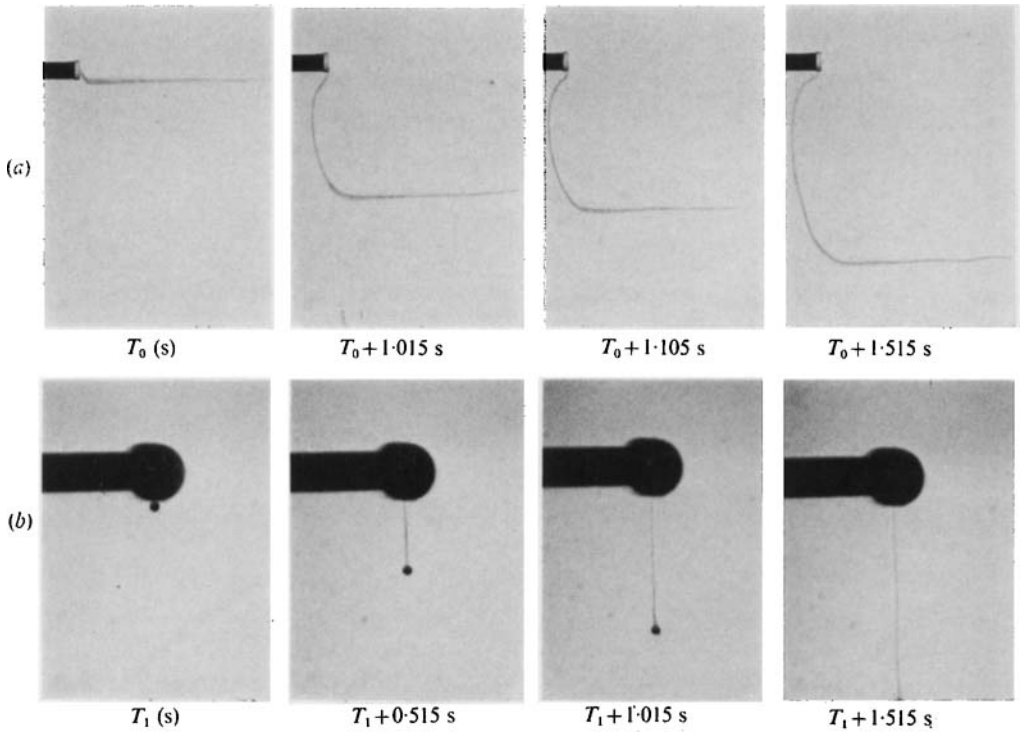

FIGURE 4. Dye traces illustrating flat velocity profile, $U_0 = 7{\cdot}49$ cm/s.
(*a*) $L_e = 6{\cdot}2$ cm. (*b*) $L_e = 4{\cdot}9$ cm.

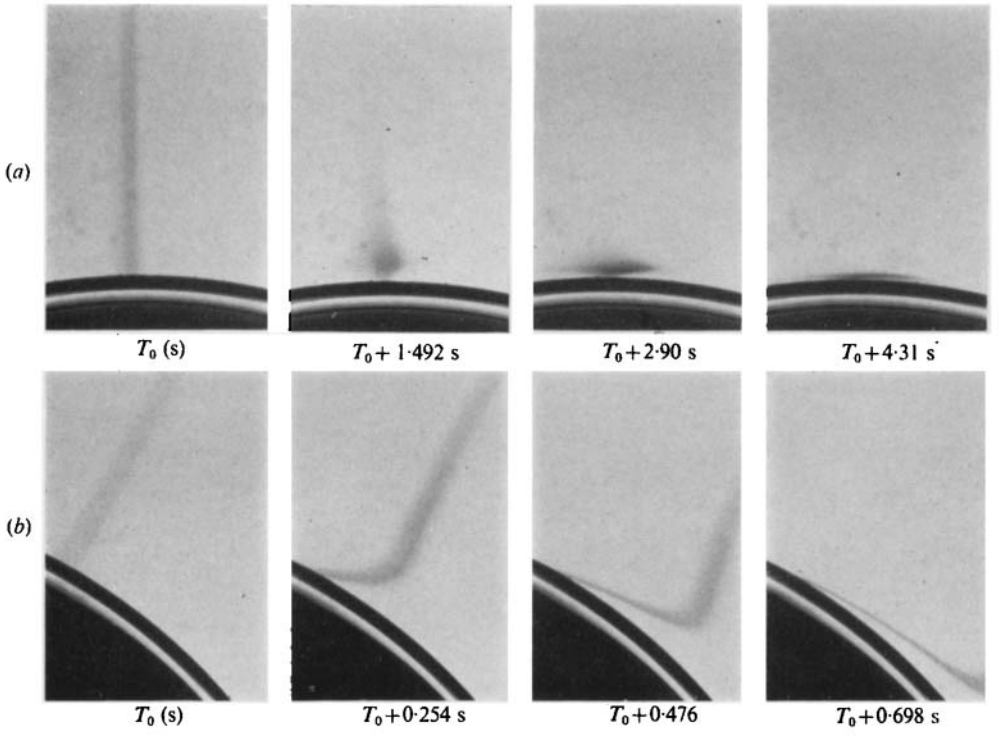

FIGURE 5. Dye traces at $Re = 760$ for 6·008 cm sphere. (*a*) $\theta = 0°$. (*b*) $\theta = 33·5°$. $L_e = 1·78$ cm.

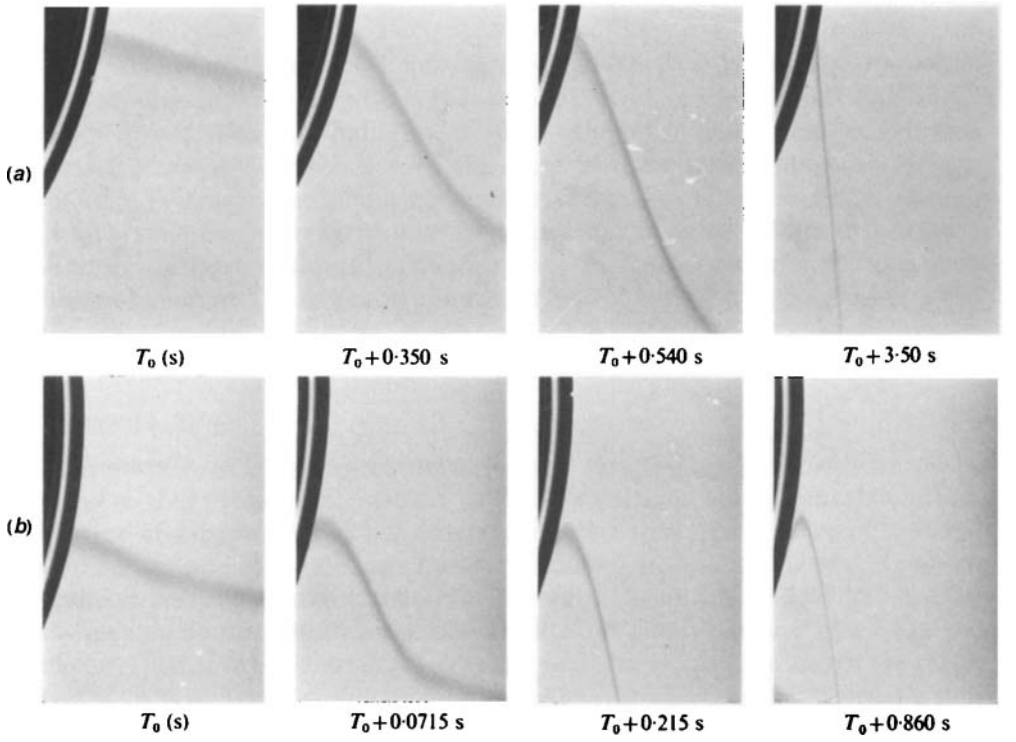

FIGURE 6. Dye traces at (*a*) Re = 760 and (*b*) Re = 2940 for 6·008 sphere; θ = 103·5°, L_c = 1·78 cm.